Electronic structure and molecular orbital study of the first excited state of the high-efficiency blue OLED material bis(2-methyl-8-quinolinolato)aluminum(III) hydroxide complex f...

ARTICLE *in* INTERNATIONAL JOURNAL OF QUANTUM CHEMISTRY · MAY 2004

Impact Factor: 1.43 · DOI: 10.1002/qua.10803

Electronic Structure and Molecular Orbital Study of the First Excited State of the High-Efficiency Blue OLED Material Bis(2-Methyl-8-Quinolinolato)Aluminum(III) Hydroxide Complex from Ab Initio and TD-B3LYP

HONG-ZE GAO,[1,2] ZHONG-MIN SU,[1] CHUN-SHENG QIN,[1] RI-GEN MO,[2] YU-HE KAN[1]

[1]*Institute of Functional Material Chemistry, Northeast Normal University, Changchun 130024, Jilin Province, China*

[2]*Fundamental Department, Chinese People's Armed Police Force Academy, Langfang 065000, Hebei Province, China*

Received 18 September 2002; accepted 26 August 2003

DOI 10.1002/qua.10803

ABSTRACT: Bis(2-methyl-8-quinolinolato)aluminum(III) hydroxide complex ($AlMq_2OH$) is used in organic light-emitting diodes (OLEDs) as an electron transport material and emitting layer. By means of ab initio Hartree–Fock (HF) and density functional theory (DFT) B3LYP methods, the structure of $AlMq_2OH$ was optimized. The frontier molecular orbital characteristics and energy levels of $AlMq_2OH$ have been analyzed systematically to study the electronic transition mechanism in $AlMq_2OH$. For comparison and calibration, bis(8-quinolinolato)aluminum(III) hydroxide complex (Alq_2OH) has also been examined with these methods using the same basis sets. The lowest singlet excited state (S_1) of $AlMq_2OH$ has been studied by the singles configuration interaction (CIS) method and time-dependent DFT (TD-DFT) using a hybrid functional, B3-LYP, and the 6-31G* basis set. The lowest singlet electronic transition ($S_0 \rightarrow S_1$) of $AlMq_2OH$ is $\pi \rightarrow \pi^*$ electronic transitions and primarily localized on the different quinolate ligands. The emission of $AlMq_2OH$ is due to the electron transitions from a phenoxide donor to a pyridyl acceptor from another quinolate ligand including C → C and O → N transference. Two possible electron transfer pathways are presented, one by carbon, oxygen, and nitrogen atoms and the

Correspondence to: Z.- M. Su, e-mail: zmsu@nenu.edu.cn

other via metal cation Al^{3+}. The comparison between the CIS-optimized excited-state structure with the HF ground-state structure indicates that the geometric shift is mainly confined to the one quinolate and these changes can be easily understood in terms of the nodal patterns of the highest occupied and lowest unoccupied molecular orbitals. On the basis of the CIS-optimized structure of the excited state, TD-B3-LYP calculations predict an emission wavelength of 499.78 nm. An absorption wavelength at 380.79 nm on the optimized structure of B3LYP/6-31G* was predicted. They are comparable to AlMq2OH 485 and 390 nm observed experimentally for photoluminescence and UV-vis absorption spectra of $AlMq_2OH$ solid thin film on quartz, respectively. Lending theoretical corroboration to recent experimental observations and supposition, the reasons for the blue-shift of AlMq2OH were revealed. Int J Quantum Chem 97: 992–1001, 2004

Key words: bis(2-methyl-8-quinolinolato)aluminum(III) hydroxide complex; ab initio; TD-DFT; electronic transition mechanism

1. Introduction

Organic light-emitting diodes (OLEDs) are currently under intense investigation for application in next-generation display technologies. OLEDs are heterojunction devices in which layers of organic transport materials are usually incorporated into devices as amorphous thin solid films. These devices normally consist of at least one hole-transport layer and one electron-transport layer forming an organic/organic heterojunction. Holes from the anode and electrons from the cathode travel through the transport layers until they form a singlet exciton that relaxes, giving rise to electroluminescence. The organic materials are chosen with close regard to their orbital energy levels, and as such the electrons are usually confined to the electron-transport layer, which, upon injection of holes, also acts as the emitting layer. Research into organic materials for use in OLEDs has been mostly focused on conjugated polymers [1, 2] or low-molecular-weight materials [3]. In 1987, Tang and VanSlyke [4] reported the first efficient low-molecular-weight OLED. Their device was constructed of two active layers and used the metaloquinolate tris(8-hydroxyquinoline)aluminum (Alq3) as the electron-transport material and emitting layer. Following the initial report, metaloquinolates have become the focus of new electroluminescent materials research [5, 6], with Alq3 being the most often used [7]. It is a green emitter with emission maximum in the range of 530 nm. For the design of a full-color red–green–black (RGB) display, high-efficiency dyes with emission in red and blue are also desired.

By tradition, a blue emitter has a lower efficiency due to its large band-gap energy, which may deter injection of electrons from the cathode. Inserting an electron-donating group at the 2- and 4-positions of the quinoline ligand can also achieve blue-shift in the emission spectrum. Kido and Iizumi reported one of the highest efficiencies (external quantum efficiency of 2.5% photo/electron) small-molecule OLEDs based on tris(4-methyl-8-quinolinolato) Al(III) complex [8]. The bluish-green emitter has a single emission peak at 506 nm. Hamada et al. reported that the gallium complex ($GaMq_2Cl$) consists of two 8-hydroxyquinaldines and one chlorine atom. The compound has a greenish blue emission with maxima at 492 and 530 nm, and its performance (maximum intensity 10.490 cd/m^2) is similar to Alq_3 [9]. A recent study proposed that a weaker metal—nitrogen in Alq_3 type complexes can also result in a shorter emission wavelength [10]. One such blue emitter without the metal—nitrogen bond reported was lithium tetra(2-methyl-8-hydroxy-quinolinato) boron ($LiBq_{m4}$) [11]. The electroluminescence (EL) spectrum for the OLED has a single emission maximum at 470 nm. The luminescence efficiency of the device is in the range of 1.3 lm/W and a maximum luminance of 6900 cd/m^2, which presents one of the highest-efficiency blue emitters reported yet with good color purity. Parallel to this latest development, bis(2-methyl-8-quinolinolato)aluminum(III) hydroxide complex ($AlMq_2OH$), a high-efficiency blue dye with a single emission maximum at 485 nm, was reported [12], which has excellent thermal stability and can be processed similar to Alq_3. The blue-shift suggests a result of two conditions: (1) The aluminum complex is trivalent in nature; and (2) steric hindrance provided by the 2-methyl groups on the 8-hydroxyquinaldine ligands weakened or prohibited the formation of Al—N bondings.

To our knowledge, there has been no theoretical study on $AlMq_2OH$ until now. To reveal the reason for the blue-shift and lend theoretical corroboration to recent experimental observations and supposition, we carried out calculations of the geometry and electronic properties of AlMq2OH in neutral state, as well as the bonding characteristics in the AlMq2OH complex. With the assistance of quantum chemical calculations, the blue-shift can be interpreted.

Given the intrinsic role that excited-state formation plays in OLED devices, the excited-state properties of AlMq2OH may be as significant as or of greater significance than the ground-state properties of this material. Chemical reactions of the excited state may deplete emissive species from operating devices, potentially yielding products that quench luminescence, thereby reducing OLED output. Therefore, it is of considerable significance to characterize the excited states of AlMq2OH.

The calculation of excited-state properties typically requires significantly more computational effort than is needed for the ground state. The configuration interaction with all singly excited determinants (CIS) is an ab initio method that provides a cost-effective, semiquantitative approach for the study of excited-state properties. Analytic geometric gradients are available for CIS, allowing the efficient investigation of excited-state structures. In the present work, the CIS method is adopted to study the first singlet excited state (S_1) of AlMq2OH. The excited-state equilibrium geometry is compared with the optimized ground-state structure. More accurate estimates of the excitation energies for AlMq2OH are computed using time-dependent density functional theory (TD-DFT) with a hybrid functional. Assisting in the interpretation of results, the comparison of the AlMq2OH results with Alq3 and bis(8-quinolinolato)aluminum(III) hydroxide complex (Alq_2OH) will show the reason for the blue-shift.

2. Methods of Calculation

All the results presented in this work were obtained at the ab initio Hartree–Fock (HF) and DFT B3LYP levels of theory by means of the Gaussian 98 program [13]. Becke's three parameters hybrid method [14] using the Lee–Yang–Parr correlation function [15] was employed for all the density functional calculations. The structure of $AlMq_2OH$ was optimized and its frontier molecular orbital characteristics and energy levels of $AlMq_2OH$ have been analyzed systematically to study the electronic transition mechanism in $AlMq_2OH$. For comparison and calibration, bis(8-quinolinolato)aluminum-(III) hydroxide complex (Alq_2OH) has also been examined by means of these methods using the same basis sets. The calculation models shown in Figures 1, A and B represent different quinoline ligands in the compound. The structures of the complexes were fully optimized using a sequence of basis sets of increasing flexibility including the split-valence 6-31G and both 6-31G* basis sets. The structures of $AlMq_2OH$ were optimized in the first singlet excited state (S_1) using configuration interaction with all singly excited determinants [16] (CIS) in the frozen-core approximation and the 6-31G* basis set. On the basis of the CIS-optimized structure of the excited state, TD-B3-LYP calculations predict an emission wavelength. And, an absorption wavelength was predicted on the optimization geometry of B3LYP/6-31G*.

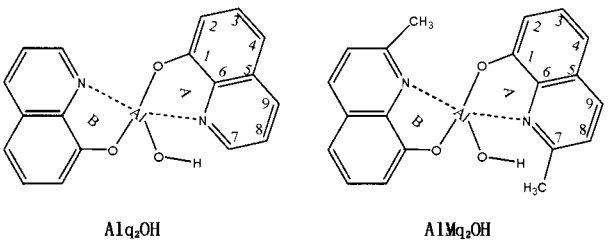

FIGURE 1. Calculation models.

3. Results and Discussion

3.1. GEOMETRIES OF STATIONARY POINTS AND ELECTRONIC STRUCTURE

3.1.1. Ground Geometries

The geometries of $AlMq_2OH$ and Alq_2OH were optimized by means of ab initio HF and DFT B3LYP methods. The main optimized parameters of each stationary point are listed in Table I; the serial numbers of atoms are shown in Figure 1.

The calculated results from different methods are consistent, that is, the results calculated are reliable. In the compound $AlMq_2OH$, the geometries from different methods are a little different. The Al—N_A bond distances are 2.0814 Å (HF/6-31G) and 2.0604 Å(B3LYP/6-31G) while in Alq_2OH the values are 2.0649 Å (HF/6-31G) and 2.0475

TABLE I
Geometric parameters optimized for $AlMq_2OH$ and Alq_2OH.

Bond distance (Å)	$AlMq_2OH$				Alq_2OH	
	HF/6-31G	HF/6-31G*	B3LYP/6-31G	B3LYP/6-31G*	HF/6-31G	B3LYP/6-31G
Al—N_A	2.0814	2.0884	2.0604	2.0704	2.0649	2.0475
Al—N_B	2.1222	2.1346	2.0948	2.1055	2.0950	2.0844
Al—O_A	1.8267	1.7967	1.8635	1.8273	1.8354	1.8693
Al—O_B	1.8256	1.7978	1.8647	1.8289	1.8346	1.8698

Å(B3LYP/6-31G). It is clear that the distance between the aluminum and nitrogen in $AlMq_2OH$ becomes longer than that in Alq_2OH owing to the introduction of methyl to the 8-hydroxyquinoline at position 2. There is the same rule in quinoline B as quinoline A. Otherwise, the angles Al-O-C1, O-C1-C6, and C1-C6-N computed in $AlMq_2OH$ become bigger than those in Alq_2OH. They made steric hindrance bigger in $AlMq_2OH$. All those mentioned above indicate that the aluminum—nitrogen becomes weaker. The bond distances of Al—N are 2.08, 2.06, and 2.13 Å (computed value, B3LYP/6-31G*) [17] and 2.04, 2.03, and 2.08 Å(experimental values) [18, 19] in alq3, compared with the Al—N bond distances computed with the B3LYP/6-31G* method in $AlMq_2OH$, which are shorter. The difference of optical luminescence and electrical luminescence between Alq3 and Gaq3 does not originate from the participation of the *d* orbital of Ga, while the structure change for the difference of metallic radius may be the key [20]. So, the Al—N distance becoming longer in $AlMq_2OH$ may be the reason for the blue-shift. Compared with both Alq_2OH and Alq3, the distance Al—O becomes shorter. This shows the aluminum—oxygen becomes stronger.

3.1.2. Charge Density Distribution

The weaker the metal—nitrogen bonding, the shorter the emission wavelength [10]. To investigate the covalent bonding of Al—N, we analyzed the charge distribution in $AlMq_2OH$ and Alq_2OH at the optimized structure with HF/6-31G and B3LYP/6-31G methods. Table II presents the results.

The charge value is different, but the tendency of results from HF/6-31G and B3LYP/6-31G is the same. The results indicate that the electrovalent bond becomes stronger and the covalent bond becomes weaker after the methyl is introduced to the Alq_2OH at position 2 of 8-hydroxyquinoline.

3.1.3. Total Energy

To reveal further the influence of introduction methyl upon the aluminum—nitrogen bond, we analyzed the energy scaling the intensity of Al—N

TABLE II
Charge distribution.

	Alq_2OH		Alq'_2OH	
	HF/6-31G	B3LYP/6-31G	HF/6-31G	B3LYP/6-31G
Al	1.8929	1.3218	1.9134	1.3461
Phenol ring (A)	−0.2226	−0.0731	−0.2523	−0.1008
Phenol ring (B)	−0.2286	−0.0750	−0.2594	−0.0984
Pyridine ring (A)	−0.1755	−0.0004	−0.2758	−0.0446
Pyridine ring (B)	−0.1917	−0.0316	−0.2904	−0.0700
O	−1.0194	−0.7564	−1.0321	−0.7655
N	−0.9199	−0.6770	−0.9560	−0.7130
—CH_3	—	—	0.1131	0.0572

bonding from results computed with the HF/6-31G and B3LYP/6-31G methods. The results are listed in Table III.

ΔE is the scaling of Al—N bonding. If the value of ΔE is positive, the bonding becomes weaker; if the value is negative, the bonding becomes stronger. The results from two methods showed that the Al—N bonding became weaker reliably.

3.1.4. Molecular Orbitals

3.1.4.1. Orbital Population. For metal chelate, the structure of the ground and excited states, electron transition, energy transfer mechanism, and so on have pronounced effects on its EL efficiency. To explore the electron transition property of $AlMq_2OH$, we made a systematic analysis of the population of the $AlMq_2OH$ molecular orbital. It was based on the stable geometric structure optimized at the ab initio HF/6-31G* and B3LYP/6-31G* levels. Meanwhile, the square sum of all kinds of atoms or molecular parts in $AlMq_2OH$ indicates the contribution of each atom or molecular moiety to one molecular orbital. All the atoms in $AlMq_2OH$ were divided into seven parts: (1) aluminum atom; (2) phenol ring, including atoms with numbers from 1–6 and mating hydrogen atoms; (3) pyridine ring, including nitrogen atom and atoms with numbers from 5–9 and mating hydrogen atoms; (4) oxygen atom; (5) nitrogen atoms; (6) hydroxy; (7) methyl. Ten orbitals were extracted from the frontier occupied orbitals and unoccupied orbitals. The results are summarized in Tables IV and V.

The result analysis demonstrates that the orbital populations coincide with the two methods, which implies that the molecular theoretical results are reliable. The electron clouds of the highest occupied molecular orbital (HOMO) is concentrated on the carbon and oxygen of the phenol ring in 8-hydroxyquinoline ring A. The electronic cloud is mainly composed of the *p* orbital ingredient and includes oxygen about 14% or so, and few *s* orbital characters are observed, with nitrogen about 6%. While in the lower occupied orbitals the contribution of the pyridine ring is primary, the electronic clouds of the lowest unoccupied molecular orbital (LUMO) are concentrated on the pyridine ring in 8-hydroxyquinoline ring B, which is mostly composed of the *p* π^* orbitals of carbon and nitrogen; the *s* orbital is little, too, including nitrogen about 10–15%. In this part higher unoccupied orbitals are from the phenol ring. In the lower occupied orbitals, as for orbitals 90, 89, 88, 87, 86, etc., the contri-

TABLE III
Total energy.

Basis set and method	Energy (a.u.)						
	E_{2q}	$E_{2q'}$	ΔE_1	E_{AlMq_2OH}	E_{AlMq_2OH}	ΔE_2	ΔE
HF/6-31G	−946.8289098	−1024.876176	−78.0472662	−1264.4577122	−1342.5123304	−78.0546182	0.007352
B3LYP/6-31G	−952.8694226	−1031.4882124	−78.6187898	−1271.3198967	−1349.9481473	−78.6282506	0.0094608

q and *q′* represent 8-hydroxyquinole and 2-methy-8-hydroxyquinole, respectively. *E* represents total energy. $\Delta E_1 = E(2q') - E(2q)$, $\Delta E_2 = E_{AlMq_2OH} - E_{Alq_2OH'}$, $\Delta E = \Delta E_1 - \Delta E_2$.

TABLE IV

Molecular orbital components of $AlMq_2OH$ (%) (HF/6-31G*).

No. orbital	Orbital energy (eV)	Al	Phenol ring A	Phenol ring B	Pyridine ring A	Pyridine ring B	O_A	O_B	N_A	N_B	OH	CH_3(A)	CH_3(B)
104	6.5607	51.6	3.5	12.5	3.7	10.7	0.6	2.8	0.7	4.4	2.9	2.8	13.9
103	6.5036	4.0	2.6	22.9	12.7	55.3	0.2	0.1	0.2	1.1	0.1	2.1	5.8
102	6.3398	52.4	10.1	4.0	12.4	13.8	2.9	1.5	4.1	0.6	1.2	0.7	7.1
101	5.7403	47.4	2.6	3.8	3.7	9.0	1.3	1.5	0.7	4.1	14.5	6.6	13.3
100	5.2706	2.0	74.4	4.8	27.9	2.5	3.5	0.3	4.8	0.6	1.4	2.4	0.9
99	5.1531	1.0	5.0	76.1	2.2	28.9	0.2	3.6	0.5	5.1	0.6	0.6	2.2
98	3.5049	0.4	62.3	0.7	69.7	0.5	0.0	0.1	0.2	0.0	0.1	2.4	0.1
97	3.3280	0.5	0.7	59.7	0.5	68.5	0.1	0.0	0.0	0.4	0.1	0.1	4.8
96	2.2439	0.6	21.3	3.8	61.8	10.7	1.0	0.6	15.6	2.8	0.4	5.1	1.0
95(LUMO)	2.1045	1.2	3.9	21.7	9.2	62.4	0.3	0.8	2.2	15.6	0.8	0.6	4.4
94(HOMO)	−7.4968	0.3	63.7	21.3	15.3	5.3	13.3	5.2	4.5	1.5	0.4	0.4	0.2
93	−7.6720	0.8	21.0	64.5	5.0	15.5	3.3	12.0	1.3	4.2	0.4	0.2	0.3
92	−8.7507	0.0	70.3	0.1	65.2	0.0	0.3	0.0	0.3	0.0	0.0	2.8	0.0
91	−8.8805	0.0	0.1	70.7	0.0	64.9	0.0	0.2	0.0	0.3	0.0	0.0	2.8
90	−10.8221	0.2	31.0	0.5	73.3	0.7	14.9	0.3	16.8	0.3	1.5	0.0	0.1
89	−10.9429	0.2	0.7	30.8	0.5	72.5	0.4	14.8	0.2	16.4	2.4	0.1	0.1
88	−11.7320	1.8	12.4	8.9	7.7	9.2	7.3	5.0	3.9	5.4	59.1	1.8	2.2
87	−11.9971	3.3	5.4	15.7	8.1	39.7	1.3	1.9	3.5	23.2	34.6	0.7	2.2
86	−12.1900	2.3	51.4	10.8	26.8	8.9	26.3	2.6	13.0	3.6	6.8	3.0	1.1
85	−12.2599	3.0	13.2	54.8	17.7	13.1	2.0	31.8	9.6	2.9	6.1	2.5	1.1

bution of nitrogen became bigger for one molecular orbital but the aluminum ingredient is still very little, occupying about 2%, which only contributes little in the deeper orbital. This shows that the aluminum—nitrogen is weaker. Figure 2 clearly exhibits the feature of the frontier orbitals.

3.1.4.2. Orbital Shapes. The interpretation of observed spectral features is greatly assisted by molecular orbital calculations, which, in addition to providing orbital energies for comparison with experiment, furnish a detailed description of orbitals, including spatial characteristics, nodal patterns, and individual atom contributions. The frontier orbital levels of $AlMq_2OH$ consist of sets of closely spaced "twosomes." The HOMOs and LUMOs of $AlMq_2OH$ largely preserve the electronic structure of the individual 8-hydroxyquinoline ligands with little contribution from the central aluminum. The least bound HOMO orbitals for $AlMq_2OH$ computed using HF/6-31G* and B3LYP/6-31G* are shown in Figure 2. The $AlMq_2OH$ orbitals are clear. The results presented here are consistent with previous results. The highest HOMO level is mainly localized on a single ligand, the a-quinolate ligand depicted in Figure 2. The LUMO orbital for 8-hydroxyquinoline and the lowest- and second lowest-energy LUMO orbitals for $AlMq_2OH$ are also shown in Figure 2. The HOMO and LUMO orbitals strongly localized on the phenoxide and pyridyl sides of the different 8-hydroxyquinoline ligands, respectively. This localization is more evident if the molecular orbitals shown in Figure 2 are plotted with smaller isosurface values.

3.1.4.3. Orbital Energies. The luminescence of metallic complex material in electroluminescence devices is due to the combination of electron and hole. The electron injected from the cathode should fill in the pyridine ring, which has become the electron potential energy container, while the hole injected from the anode should concentrate on the phenol ring, which has become the hole potential energy container. So, the energy of LUMO has an effect on turn-on voltage. The LUMO energies of Alq3 and $AlMq_2OH$ are 1.8583 [21] and 1.9410 eV computed at the HF/6-31G level, which indicates that $AlMq_2OH$ has a higher energy barrier for charge injection and so $AlMq_2OH$ has a slightly higher turn-on voltage. The result is consistent with the experiment [12].

TABLE V

Molecular orbital components of $AlMq_2OH$ (%) (B3LYP/6-31G*).

No. orbital	Orbital energy (eV)	Al	Phenol ring A	Phenol ring B	Pyridine ring A	Pyridine ring B	O_A	O_B	N_A	N_B	OH	CH_3(A)	CH_3(B)
104	2.5612	1.2	1.3	21.2	3.5	65.5	0.0	0.0	0.1	0.6	0.9	0.9	8.2
103	2.4812	7.6	23.5	7.0	29.8	25.5	0.5	2.6	1.7	0.7	0.8	7.0	2.2
102	2.3465	12.4	4.7	30.5	5.6	37.9	2.4	1.3	1.3	4.2	1.3	0.2	11.1
101	1.9296	31.3	3.7	4.3	5.8	11.3	1.9	1.8	1.7	4.3	21.1	6.5	17.0
100	0.9641	0.4	81.4	1.8	30.2	1.1	4.7	0.1	6.0	0.3	0.4	1.5	0.8
99	0.8430	0.5	1.8	82.3	0.8	29.8	0.2	4.9	0.2	6.0	0.4	0.5	1.5
98	−0.3157	0.2	60.3	0.4	69.9	0.3	0.0	0.0	0.1	0.0	0.1	2.3	0.1
97	−0.4757	0.3	0.4	58.5	0.3	69.9	0.0	0.0	0.0	0.2	0.1	0.1	3.3
96	−1.5141	0.6	23.0	2.3	68.4	5.7	1.5	0.7	19.1	1.8	0.6	4.4	0.5
95(LUMO)	−1.6730	1.0	2.4	23.1	4.8	68.9	0.4	1.3	1.2	19.2	0.8	0.2	4.3
94(HOMO)	−5.3033	0.4	62.9	22.8	13.9	5.4	19.1	7.9	3.1	1.1	1.3	0.5	0.5
93	−5.4976	1.5	22.6	63.6	5.0	14.1	5.2	17.1	1.0	2.8	1.1	0.3	0.4
92	−6.6900	0.1	66.6	0.1	61.0	0.1	0.2	0.0	0.2	0.0	0.2	4.6	0.0
91	−6.8309	0.1	0.1	67.3	0.0	60.4	0.0	0.2	0.0	0.2	0.2	0.0	4.4
90	−7.0851	3.4	6.8	5.7	2.2	2.7	3.2	2.4	0.9	1.3	75.2	1.8	3.1
89	−7.5610	8.0	4.4	12.9	6.3	16.3	1.7	4.9	1.3	9.0	56.9	0.6	0.4
88	−7.7607	5.1	51.5	21.7	18.7	9.0	32.5	13.7	2.6	2.5	4.9	0.4	0.8
87	−7.8508	3.3	36.5	8.4	38.5	15.5	22.0	4.0	9.3	5.0	4.2	0.8	0.4
86	−7.9820	6.0	19.3	45.8	14.5	19.5	12.0	30.0	6.9	8.5	0.3	2.0	2.0
85	−8.0103	3.0	11.4	38.4	8.0	42.5	6.7	21.7	1.9	8.8	4.6	0.4	0.8

3.2. $S_0 \rightarrow S_1$ Excitation Energy and the S_1 Excited-State Structure

Experimental investigations of the excited-state properties of $AlMq_2OH$ have been made on the photoabsorption, photoluminescence, and electroluminescence of this OLED material [12]. Inspection of the absorption and emission spectra from $AlMq_2OH$ in condensed-phase systems shows that both the EL and PL spectrum have a similar shape, with a single emission maximum at 485 nm. The

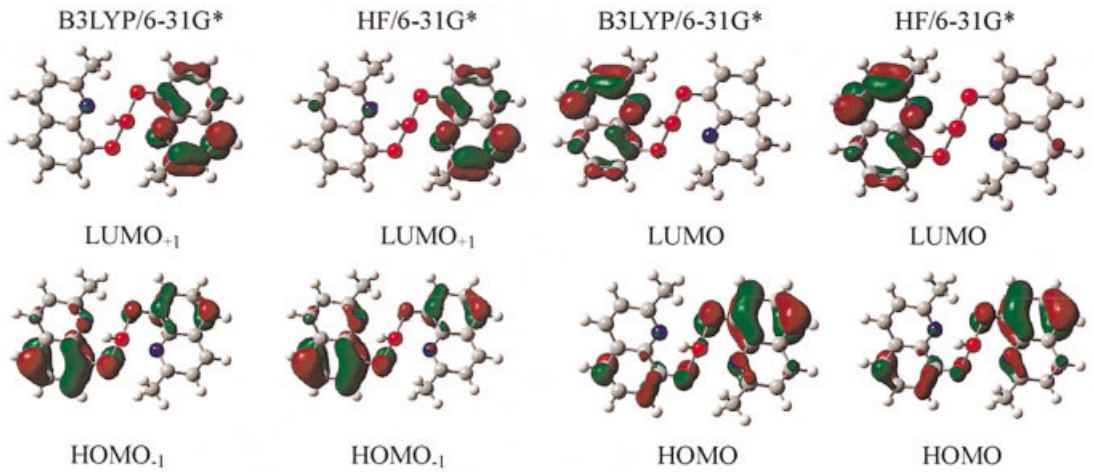

FIGURE 2. Molecular orbital surfaces of the HOMO, second highest-energy molecular orbital ($HOMO_{-1}$), LUMO, and second lowest-energy molecular orbital ($LUMO_{+1}$) of $AlMq_2OH$.

results presented here support the localized nature of the orbitals involved in the lowest-energy electronic transitions in $AlMq_2OH$. The lowest electronic transitions are $\pi \rightarrow \pi^*$ transitions in the different quinolate rings, involving partial charge transfer from the phenoxide side to the pyridyl side. There are two ways of electron transfer: (1) the direct transition through carbon in quinoline ring; (2) through the metal ion, which is not only a support but also a bridge of electron transfer. These may be the reasons for the blue-shift of $AlMq_2OH$.

3.2.1. $S_0 \rightarrow S_1$ Vertical Excitation Energy

In the present study, configuration interaction with all single (CIS) excited determinants is employed to study the lowest-energy singlet excited state (S_1) of $AlMq_2OH$. CIS represents for excited states a general zeroth-order method, just as HF is for the ground state of molecular systems. Besides being relatively inexpensive, permitting it to be applied to large molecules such as Alq3, analytic derivatives are available for CIS allowing the efficient calculation of excited-state structures and properties [16, 22].The vertical excitation energies of $AlMq_2OH$ computed using CIS are presented. Comparison of the CIS/6-31G* vertical excitation energies of $AlMq_2OH$ with the experimental values shows that the CIS calculations clearly overestimate the lowest excitation energies by ca. 0.4 eV. CIS theory is known to overestimate electronic excitation energies due to the neglect of the effects of electron correlation and higher-order excitations. To investigate the effect of electron correlation on the computed energies, calculations using TD-DFT and the hybrid density functional B3-LYP were carried out with the 6-31G* basis set for $AlMq_2OH$, so direct comparison with the CIS/6-31G* results can be made. For $AlMq_2OH$, the TD-DFT calculations were carried out at the B3LYP/6-31G*-optimized structure. The excitation energy calculated is 3.2560 eV (380.79 nm), which is approximate to the experiment result [12]. Recent work by Stratmann et al. [23] has shown that TD-DFT yields significantly better results than those provided by HF-based methods such as the random phase approximation (RPA) or CIS yet is similar in cost. Comparison of the TD-B3-LYP excitation energies with the experimental values shows improved agreement over the CIS results. Pople and coworkers [16] observed that with the CIS method the use of basis sets that included significant polarization resulted in a larger overestimation of excitation energies; however, the excited-state potential energy surface was found to be more accurate. This behavior was attributed to the fact that these functions lower the ground-state reference energies to a greater extent than do the excited-state energies.

3.2.2. S_1 Excited-State Structure

Studies of the excited-state properties for a number of molecules using the CIS method have found that, despite the tendency of CIS to overestimate electronic transition energies, the excited-state potential energy surface can often be quite accurate, as evidenced by comparison of equilibrium excited-state structures with experiment [16]. Experimental studies of $AlMq_2OH$ have observed a large shift between the optical absorption spectra and emission spectra, which is thought to arise from significant differences between the ground- and excited-state structures. To investigate the geometry change associated with electronic excitation to the lowest-energy singlet excited state ($S_0 \rightarrow S_1$), the geometry of $AlMq_2OH$ was optimized at the CIS/6-31G* level of theory in the S_1 state for comparison with the HF/6-31G* ground-state structure. Table VI presents the optimized ground- and excited-state bond lengths for $AlMq_2OH$. Note that positive and negative values in the percentage difference columns indicate bond elongation and contraction in the excited state, respectively. Comparison of the excited- and ground-state geometries for A- and B-quinolates in $AlMq_2OH$ indicates that the structural shift is predominantly localized on the B-quinolate. The B-quinolates in $AlMq_2OH$ are practically unaffected except for changes in the Al—O and Al—N bond lengths.

3.2.3. Orbital Analysis

The lowest-energy singlet transition for $AlMq_2OH$ at the CIS/6-31G* level of theory involves transitions from the least bound HOMO orbital to the lowest- and the second lowest-energy LUMO orbitals with about equal weight. The least bound HOMO orbital of $AlMq_2OH$ is mainly localized on the A-quinolate, but the LUMOs also have contributions from the B rings and the localized nature of the electronic excitation is clear. The observed geometry relaxation in $AlMq_2OH$ can be rationalized by consideration of the nodal patterns of the HOMO and LUMO orbitals in Figure 2. The lowest-energy singlet excitation ($S_0 \rightarrow S_1$) is mainly HOMO $\rightarrow$ LUMO in character. The LUMO has

TABLE VI

HF/6-31G* ground-state and CIS/6-31G* excited-state bond lengths for the A- and B-quinolate ligands in $AlMq_2OH$.

Bond distance (Å)	HF/6-31G*		CIS/6-31G*		$(R_{CIS}-R_{HF})/R_{HF} \times 100\%$	
	A	B	A	B	A	B
Al—O	1.7967	1.7978	1.8712	1.7905	4.15	−0.41
Al—N	2.0884	2.1346	1.9987	2.1874	−4.30	2.47
O—Cl	1.3152	1.3139	1.2715	1.3135	−3.32	−0.03
C1—C2	1.3660	1.3671	1.4339	1.3674	4.97	0.02
C2—C3	1.4162	1.4150	1.3600	1.4143	−3.97	−0.05
C3—C4	1.3610	1.3618	1.4222	1.3622	4.50	0.03
C4—C5	1.4190	1.4179	1.4029	1.4175	−1.13	−0.03
C5—C6	1.3926	1.3936	1.4105	1.3942	1.29	0.04
N—C6	1.3570	1.3579	1.3360	1.3579	−1.55	0.00
C7—N	1.3043	1.3033	1.3816	1.3028	5.93	−0.04
C7—C8	1.4185	1.4193	1.3650	1.4202	−3.77	0.06
C8—C9	1.3595	1.3590	1.4139	1.3584	4.00	−0.04
C1—C6	1.4258	1.4261	1.4289	1.4250	0.22	−0.08
C5—C9	1.4159	1.4168	1.4010	1.4170	−1.05	0.01
C7—C(CH_3)	1.5038	1.5054	1.4975	1.5060	−0.42	0.04
Al—O(OH)	1.7364		1.7317		−0.27	

nodes across the C1—C2 and C3—C4 bonds in the phenol ring and there has been bonding in the pyridyl ring of quinoline A, but the HOMO is bonding in corresponding regions and has no bonding in the pyridyl ring of quinoline A. Therefore, one would expect elongation of these bonds and contraction in some region of the pyridyl ring; Table VI shows that these bonds are in fact considerably longer and shorter in the excited state, respectively.

3.2.4. $S_1 \rightarrow S_0$ Emission Energy

The CIS calculations for $AlMq_2OH$ also provide an estimate of the relaxed emission energy from the optimized CIS excited-state structure to the HF ground state ($S_1 \rightarrow S_0$). TD-B3-LYP/6-31G* calculations were carried out for $AlMq_2OH$ at the CIS/6-31G*-optimized excited-state structure to obtain more accurate estimates of the emission energy. With TD-B3-LYP, the emission energy is predicted to be ca. 2.4807 eV, corresponding to emission at ca. 499.78 nm, which is in much closer agreement with the energy of the experimental photoluminescence and electroluminescence emission observed in condensed phase at ca. 485 nm (2.5616 eV) [12].

4. Conclusions

The first singlet excited state (S_1) of $AlMq_2OH$ has been studied using the CIS/6-31G* and TD-B3-LYP/6-31G* levels of theory. The electronic excitation and structural relaxation in the excited state for $AlMq_2OH$ have been interpreted in terms of the nature and nodal characteristics of the HOMO and LUMO. The correlation between the electronic excitation and the structural relaxation in the excited state for $AlMq_2OH$ has been made. The $S_0 \rightarrow S_1$ excitation is found to be mainly localized on the different quinolate ligands; this may be the main reason for the blue-shift of $AlMq_2OH$. At the TD-B3-LYP level of theory, the calculated wavelength for emission agree very well with the experiment. The reason for blue-shift in $AlMq_2OH$ from Alq3 can be interpreted from theoretical results.

References

1. Burroughes, J. H.; Bradley, D. D. C.; Brown, A. R.; Marks, R. N.; Mackay, K.; Friend, R. H.; Burns, P. L.; Holmes, A. B. Nature 1990, 347, 539.
2. Friend, R. H.; Gymer, R. W.; Holmes, A. B.; Burroughes, J. H.; Marks, R. N.; Taliani, C.; Bradley, D. D. C.; Dos Santos,

D. A.; Bredas, J. L.; Logdlund, M.; Salaneck, W. R. Nature 1999, 397, 121.

3. Mitsche, U.; Bauerfe, P. J Mater Chem 2000, 10, 1471.
4. Tang, C. W.; VanSlyke, S. A. Appl Phys Lett 1987, 51, 913.
5. Hamada, Y. IEEE Trans Electron Devices 1997, 44, 1208.
6. Chen, C. H.; Shi, J. Coord Chem Rev 1998, 171, 161.
7. VanSlyke, S. A.; Chen, C. H.; Tang, C. W. Appl Phys Lett 1996, 69, 2160.
8. Kido, J.; Iizumi, Y. Chem Lett 1997, 10, 963.
9. Hamada, Y.; Kanno, H.; Sano, T.; Fujii, H.; Nishio, Y.; Takahashi, H.; Usuki, T.; Shibata, K. Appl Phys Lett 1998, 72, 1939.
10. Chen, C. H.; Shi, J. M. Coord Chem Rev 1998, 171, 161.
11. Tao, X. T.; Suzuki, H.; Wada, T.; Miyata, S.; Sasabe, H. J Am Chem Soc 1999, 121, 9447.
12. Leung, L. M.; Lo, W. Y.; So, S. K.; Lee, K. M.; Choi, W. K. J Am Chem Soc 2000, 122, 5640.
13. Frisch, M. J.; Trucks, G. W.; Schlegel, H. B.; Scuseria, G. E.; Robb, M. A.; Cheeseman, J. R.; Zakrzewski, V. G.; Montgomery, J. A.; Stratmann, R. E.; Burant, J. C.; Dapprich, S.; Millam, J. M.; Daniels, A. D.; Kudin, K. N.; Strain, M. C.; Farkas, O.; Tomasi, J.; Barone, V.; Cossi, M.; Cammi, R.; Mennucci, B.; Pomelli, C.; Adamo, C.; Clifford, S.; Ochterski, J.; Petersson, G. A.; Ayala, P. Y.; Cui, Q.; Morokuma, K.; Malick, D. K.; Rabuck, A. D.; Raghavachari, K.; Foresman, J. B.; Cioslowki, J.; Ortiz, J. V.; Stefanov, B. B.; Liu, G.; Liashenko, A.; Piskorz, P.; Komaromi, I.; Gomperts, R.; Martin, R. L.; Fox, D. J.; Keith, T.; Al-Laham, M. A.; Peng, C. Y.; Nanayakkara, A.; Gonzalez, C.; Challacombe, M.; Gill, P. M. W.; Johnson, B. G.; Chen, W.; Wong, M. W.; Andres, J.; Head-Gordon, M.; Replogle, E. S.; Pople, J. A. Gaussian 98, Revision A.9; Gaussian, Inc.: Pittsburgh, PA, 1998.
14. Becke, A. D. J Chem Phys 1993, 98, 5648.
15. Lee, C.; Yang, W.; Parr, R. G. Phys Rev B 1988, 37, 785.
16. Foresman, J. B.; Head-Gordon, M.; Pople, J. A.; Frisch, M. J. J Phys Chem 1992, 96, 135.
17. Richard, L. M.; Joel, D. K. Phys Rev B 2000, 61, 15804.
18. Fujii, I.; Hirayama, N.; Ohtani, J.; Kodama, K. Anal Sci 1998, 12, 153.
19. Schmidbaur, H.; Lettenbauer, J.; Wilkinson, D. L.; Muller, G.; Kumberger, O. Z Naturforsch B 1991, 46, 901.
20. Su, Z. M.; Gao, H. Z.; Cheng, H.; Chu, B.; Cheng, L. H.; Wang, R. S.; Wang, Y.; Shen, J. C. Sci China B 2000, 43, 658.
21. Su, Z. M.; Cheng, H.; Gao, H. Z.; Sun, S. L.; Chu, B.; Wang, R. S.; Wang, Y. Chem J Chin Univ 2000, 21, 1416.
22. Foresman, J. B.; Schlegel, H. B. In Recent Experimental and Computational Advances in Molecular Spectroscopy; Gausto, R.; Hollas, J. M., Eds.; Kluwer Academic: Dordrecht, The Netherlands, 1993; p 11, 406.
23. Stratmann, R. E.; Scuseria, G. E.; Frisch, M. J. J Chem Phys 1998, 109, 8218.